Mesoscale simulations of granular materials with peridynamics

Christopher J. Lammi and Tracy J. Vogler

Citation: AIP Conf. Proc. **1426**, 1467 (2012); doi: 10.1063/1.3686559
View online: http://dx.doi.org/10.1063/1.3686559
View Table of Contents: http://proceedings.aip.org/dbt/dbt.jsp?KEY=APCPCS&Volume=1426&Issue=1
Published by the American Institute of Physics.

MESOSCALE SIMULATIONS OF GRANULAR MATERIALS WITH PERIDYNAMICS

C. J. Lammi[1] and T. J. Vogler[2]

[1]*Georgia Institute of Technology, George W. Woodruff School of Mechanical Engineering, 801 Ferst Dr. NW, Atlanta, GA 30332*
[2]*Sandia National Laboratories, Livermore CA 94550*

Abstract. The dynamic behavior of granular materials can be quite complex due to phenomena that occur at the scale of individual grains. For this reason, mesoscale simulations explicitly resolving individual grains with varying degrees of fidelity have been used to gain insight into the physics of granular materials. The vast majority of these simulations have, to date, been performed with Eulerian codes, which do a poor job of resolving fracture and grain-to-grain interactions. To address these shortcomings, we utilize a peridynamic modeling framework to examine the roles of fracture and contact under planar shock and other loading conditions. Peridynamics is a mesh-free Lagrangian technique based on an integral formulation to better enable simulations involving fracture.

Keywords: Granular materials, peridynamics, mesoscale modeling
PACS: 45.70.-n, 79.20.Ap.

INTRODUCTION

Continuum-level dynamic models for granular materials such as the P-α [1] and P-λ [2] models homogenize material response and account for fine scale mechanics using empirical parameters. Insight into the fine scale behavior relevant to the dynamic response of granular materials via computational mesoscale modeling at the scale of grains was pioneered by Benson [3] and later explored using Eulerian hydrodynamic calculations [4-5]. While the results of these studies have shown general agreement with experiment, the Eulerian framework lacks grain-to-grain contact dynamics and fracture. These phenomena are likely to be important in the dynamic behavior of granular materials.

To study the role of fracture and grain-to-grain contact, we explore here an alternative numerical approach, peridynamics. Peridynamics is non-local, integral reformulation of the governing laws of mechanics proposed by Silling [6]. The mechanical response of a peridynamic material point is dependent on the current deformation state and deformation history of all material points within a given distance, or horizon. In the past decade it has been applied to a variety of dynamic problems of both brittle and ductile materials involving fracture. The discontinuities in dis-placement (and thus strain) which result from the initiation of cracks are typically difficult using classical, local constitutive models without the addition of, often aphysical, numerical techniques. Peridynamics is adept at handling discontinuities since it relies on the evaluation of integrals rather than partial derivatives.

COMPUTATIONAL APPROACH

Two-dimensional, plane strain, mesoscale models were constructed of size 1 mm × 2 mm containing 56% volume fraction of 32 μm diameter grains. Grains were assigned the mechanical properties of quartz sand. Peridynamic material points were uniformly distributed within each grain with a spacing of 4 μm, and the peridynamic

Shock Compression of Condensed Matter - 2011
AIP Conf. Proc. 1426, 1467-1470 (2012); doi: 10.1063/1.3686559

horizon was set uniformly throughout the model to approximately 12 μm. Three material responses were considered, linear-elastic, linear-elastic with fracture in tension, and elastic-perfectly plastic with fracture in tension. When plasticity was enabled, the specified flow stress was 5 GPa and the equivalent plane strain fracture toughness was varied from 0.6 to 2.5 MPa√m. Studies measuring the plain strain fracture toughness of fused and crystalline quartz have reported values between 0.5-1.0 MPa√m. No-displacement boundary conditions were applied to the top, bottom, and right of the model; a driver was simulated using a velocity boundary condition on the left. Driver velocity was varied from 200-600 m/s. The configuration of the analysis is shown in Fig 1. Calculations were performed in the parallel, explicit, peridynamic solver EMU. Within EMU, the integrals of peridynamics are discretized using material point, or nodal, masses connected by linear or non-linear springs (bonds).

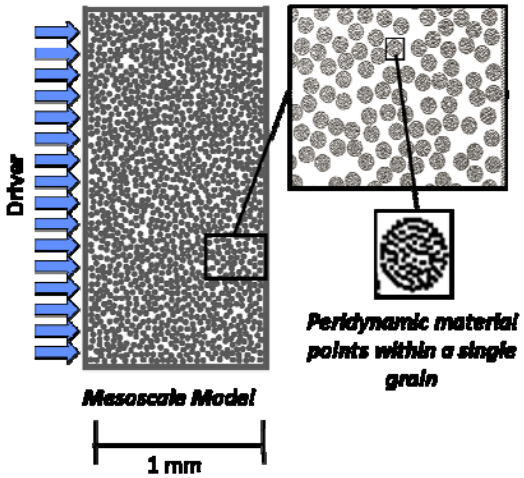

Figure 1. Configuration of the mesoscale model used in calculations.

The behavior of each mesostructure was evaluated in terms of longitudinal and transverse velocity fields, damage, and Hugoniot response. Damage is evaluated in the peridynamic framework on a scale of 0 to 1, where 0 represents a peridynamic material point has no broken bonds with other points in its horizon while 1 represents all bonds have been broken.

RESULTS AND DISCUSSION

Representative visualizations of the longitudinal and transverse velocity fields 1 μs after driver motion begins are shown in Fig 2(a)-(c) and 2(d)-(f) respectively for the three mechanical behaviors modeled.

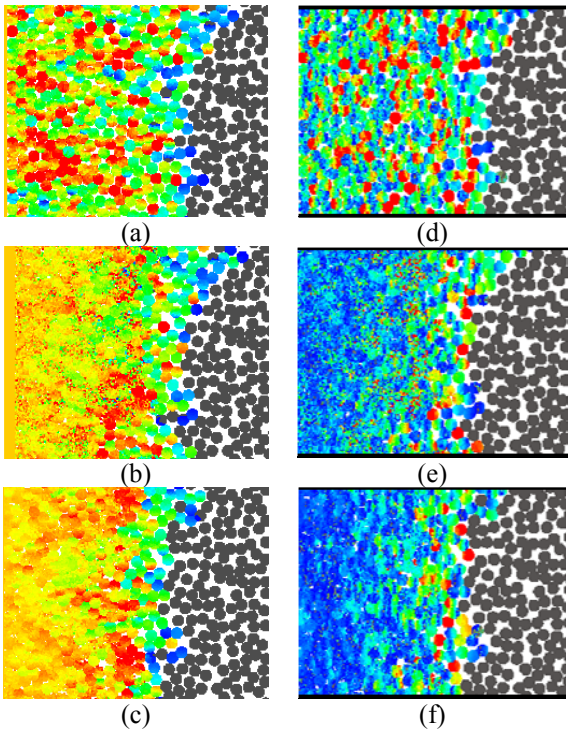

Figure 2. Longitudinal and transverse velocity fields at 1 μs: (a) longitudinal, linear-elastic grains; (b) longitudinal, linear-elastic fracture grains (K_{IC}=0.6 MPa√m); (c) longitudinal, linear-elastic fracture grains with plasticity; (d) transverse, linear-elastic grains; (e) transverse, linear-elastic fracture grains; and (f) transverse, linear-elastic fracture grains with plasticity.

TABLE 1. Calculated Hugoniot response for grains that are linear-elastic or linear-elastic with fracture.

Material Behavior	u_p, m/s	U_s, m/s	ρ_H, kg/m^3	σ_H, GPa
Linear-elastic	200	664	2124	0.197
	400	1159	2266	0.688
	600	1455	2525	1.296
Linear-elastic, fracture K_{IC}=0.6 MPa$\sqrt{m}$	200	679	2104	0.202
	400	1090	2344	0.647
	600	1458	2522	1.298

Analysis of the distribution of material point velocities reveals that:

1. Fracture and plasticity increase the homogeneity of the velocity fields;
2. Transverse momentum, and thus energy of scattering decreases with the addition of fracture and decreases further with the addition of plasticity.

It was calculated that the kinetic energy of scattering decreased by 10% by allowing fracture and 50% by allowing plastic flow in compression.

Calculation of the shock velocity for each mesoscale simulation was performed by recording the time and location at which a grain "joined" the shock front. Representative displacement-time records for linear-elastic grains are shown in Fig. 3 for driver velocities of 200, 400, and 600 m/s. The slope of a linear regression through the scatter plot of the data yields the shock velocity.

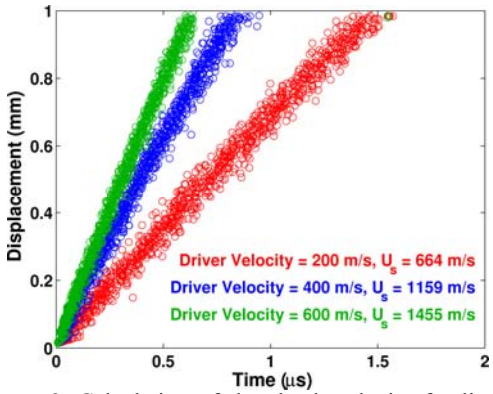

Figure 3. Calculation of the shock velocity for linear-elastic grains with driver velocities of 200, 400, and 600 m/s.

A linear relationship was found between the particle and shock velocities (u_p-U_s), shown in Fig. 4, in agreement with experiments to determine the equation of state of granular materials [7]. It was found that the EMU calculations resulted in slopes approximately 10% lower than what was found in experiment. Knowledge of both the particle and shock velocities allows calculation of all remaining Hugoniot parameters. Hugoniot stresses and densities were calculated using conservation of momentum yielding,

$$\sigma_H = \rho_{00} U_s u_p , \tag{1}$$

and conservation of mass yielding,

$$\rho_H = \rho_{00} \frac{U_s}{U_s - u_p} , \tag{2}$$

where U_s and u_p are the shock and particle velocities, ρ_{00} and ρ_H are the initial (1,480 kg/m^3) and Hugoniot densities, and σ_H is the Hugoniot stress. The Hugoniot compaction curve from EMU calculations and experiment is shown in Fig. 5 and a summary of the calculated Hugoniot densities and stresses is presented in Table 1.

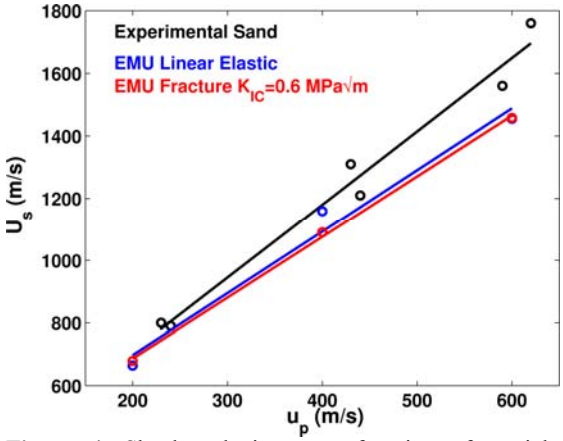

Figure 4. Shock velocity as a function of particle velocity for grains with linear-elastic and linear-elastic fracture properties compared to experiment.

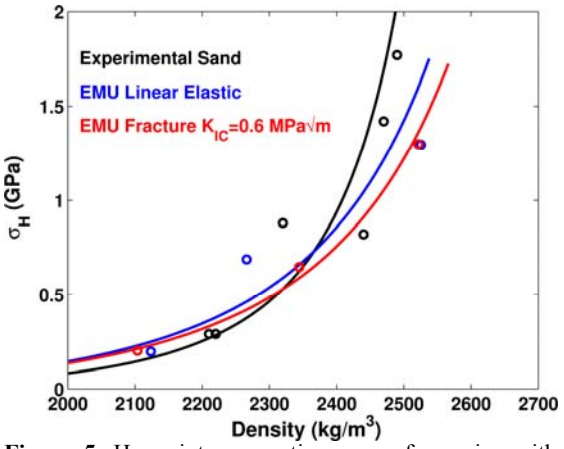

Figure 5. Hugoniot compaction curve for grains with linear-elastic and linear-elastic fracture properties compared to experiment.

The greatest asset of the peridynamic framework used in this analysis in regards to shock compression of granular materials is the ability to capture the grain to grain contact dynamics as well as fracture and comminution of material. Accumulated damage in structures with circular and random shaped grains 1 μs after impact is shown in Fig. 6. It is observed that 32% and 71% of the shock front is completely pulverized in these two cases, respectively. More work is needed to understand the effect of particle morphology on the compaction of these materials.

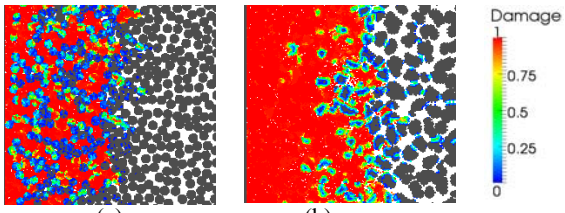

(a) (b)

Figure 6. Accumulated damage for (a) circular, and (b) random shaped, grains with linear-elastic fracture material properties.

CONCLUSIONS

The peridynamic framework has been used to study the planar compaction of granular ceramics. It offers more physically realistic treatment of grain to grain contact and fracture than the previously used Eulerian frameworks. Hugoniot data for continuum level models was reasonably approximated using this new approach while accounting for the aforementioned phenomena. In addition to agreement with experiment, the EMU calculations additionally predict large volume fractions of comminuted and completely pulverized material, which agrees with experimentation. Future studies will explore the effects of particle morphology on the calculated Hugoniot response and more complicated loading conditions.

ACKNOWLEDGEMENTS

Sandia National Laboratories is a multi-program laboratory managed and operated by Sandia Corporation, a wholly owned subsidiary of Lockheed Martin Corporation, for the U.S. Department of Energy's National Nuclear Security Administration under contract DE-AC04-94AL85000.

REFERENCES

1. Hermann, H., "Constitutive equation for the dynamic compaction of ductile porous materials," J. Appl. Phys. **40**, pp 2490-2499 (1969).
2. Grady, D. E. and Winfree, N. A., "A computational model of polyurethane foam," In: Staudhammer, K.P., Murr, L.E., and Meyers, M.A. ed, *Fundamental issues and applications of shock-wave and high-strain-rate phenomena, Proceedings of EXPLOMET*, pp 485-491 (2001).
3. Benson, D. J., "The numerical simulation of the dynamic compaction of powders," In: Davison, L., Horie, Y., and Shahinpoor, M. ed., *High-Pressure Shock Compression of Solids IV: Response of Highly Porous Solids to Shock Loading,* N.Y., pp 233-255 (1997).
4. Borg, J. P. and Vogler, T. J., "Mesoscale calculations of the dynamic behavior of a granular ceramic," Int. J. Solids Struct. **45**, pp 1676-1696 (2008).
5. Borg, J. P. and Vogler, T. J., "Aspects of simulating the dynamic compaction of a granular ceramic," Model. Simul. Mater. Sc. **17**, pp 1676-1696 (2009).
6. Silling, S. A., "Reformulation of elasticity theory for discontinuities and long-range forces," J. Mech. Phys. Solids **48**, pp 175-209 (2000).
7. Brown, J. L., et al., "Dynamic compaction of sand," AIP Conf. Proc. **955**, pp 1363-1366 (2007).